Quantum-chromodynamic predictions for direct photons in e^+e^- collisions

Ken Sasaki*
Stanford Linear Accelerator Center, Stanford University, Stanford, California 94305
(Received 13 April 1981)

We analyze the direct photon production in e^+e^- collisions in quantum chromodynamics using the cut-vertex formalism and the renormalization-group method. The two-loop anomalous dimensions of timelike cut vertices are calculated from the two-loop parton decay probability functions. The moments of the transverse structure function $\overline{W}_T^\gamma$ are calculated up to the next-to-leading order. The nonleading corrections to $\overline{W}_T^\gamma$ turn out to be large, and even larger than those to the photon structure function F_2^γ in photon-photon scattering. Also, the moments of the longitudinal structure function $\overline{W}_L^\gamma$ are calculated in the leading order. The corrections are found to be small.

I. INTRODUCTION

For some time it has been emphasized that the measurement of the photon structure function in high-energy e^+e^- colliding-beam experiments should provide a good test of quantum chromodynamics (QCD). Because of the pointlike nature of the photon, definite predictions have been obtained for the photon structure functions in the leading and the next-to-leading orders of asymptotic freedom.[1-5] The pointlike nature of the photon also leads to precise predictions for many processes involving real photons.[3]

One such process is direct photon production in e^+e^- collisions as shown in Fig. 1,

$$e^+e^-\to\gamma^*(q)\to\gamma_{\rm direct}(p)+\text{hadrons}(\mathcal{C}=+)\,. \quad (1.1)$$

Here the virtual photon with momentum q is far off shell (large $q^2>0$) and the observed photon having momentum p is "direct," which means that it is not a decay product of radiatively decaying hadrons. The unobserved hadrons have charge conjugation $\mathcal{C}=+$.

If we define the *timelike* photon structure functions $\overline{W}_1^\gamma$ and W_2^γ as[6]

$$\begin{aligned}\overline{W}^\gamma_{\mu\nu}=&-\frac{1}{4\pi}\iiint d^4x\,d^4y\,d^4z\,e^{iq\cdot z}e^{ip\cdot(y-x)}\\&\times\langle 0|\overline{T}(J_\rho(x)J_\mu(z))T(J^\rho(y)J_\nu(0))|0\rangle\\=&\left(-g_{\mu\nu}+\frac{q_\mu q_\nu}{q^2}\right)\overline{W}_1^\gamma(p\cdot q,q^2)\\&+\left(p_\mu-\frac{p\cdot q}{q^2}q_\mu\right)\left(p_\nu-\frac{p\cdot q}{q^2}q_\nu\right)\overline{W}_2^\gamma(p\cdot q,q^2)\end{aligned} \quad (1.2)$$

with $\overline{T}$ representing anti-time-ordered products, then the cross section for the direct photon production can be written as

$$\frac{d\sigma}{dz\,d\Omega}=\frac{3\alpha}{4}\sigma_0 z\left[2\overline{W}_1^\gamma(z,q^2)+\sin^2\theta\,\frac{\nu^2}{q^2}\overline{W}_2^\gamma(z,q^2)\right]. \quad (1.3)$$

Here $\nu=p\cdot q$, $z=2\nu/q^2$, θ is the angle between the photon momentum and the e^+e^- collision axis, and

$$\sigma_0=\frac{4\pi\alpha^2}{3q^2} \quad (1.4)$$

is the total cross section for $e^+e^-\to\mu^+\mu^-$, with $\alpha=e^2/4\pi$ being the electromagnetic coupling constant. In terms of the transverse and longitudinal structure functions such as

$$\overline{W}_T^\gamma=\overline{W}_1^\gamma \quad (1.5)$$

and

$$\overline{W}_L^\gamma=\overline{W}_1^\gamma+\frac{\nu^2}{q^2}\overline{W}_2^\gamma\,, \quad (1.6)$$

we can rewrite the cross section (1.3) as

$$\begin{aligned}\frac{d\sigma}{dz\,d\Omega}=\frac{3\alpha}{4}\sigma_0 z[&\overline{W}_T^\gamma(z,q^2)(1+\cos^2\theta)\\&+\overline{W}_L^\gamma(z,q^2)(1-\cos^2\theta)]\,.\end{aligned} \quad (1.7)$$

Direct photon production in e^+e^- collisions was first studied in the parton model (PM) by Walsh and Zerwas.[6] Evaluating the s-channel discontinuity of the box diagrams in Fig. 2, they obtain

$$\overline{W}_T^\gamma|_{\rm PM}=\alpha^2\delta_\gamma 4\,\frac{1+(1-z)^2}{z^2}\ln\frac{q^2(1-z)}{m_q^2} \quad (1.8)$$

and

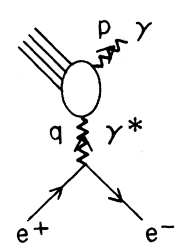

FIG. 1. Direct production of photons in e^+e^- collisions. The observed photons are assumed not to be radiative decay products of hadrons.

$$\bar{W}_L^\gamma\big|_{\rm PM} = \alpha^2\delta_\gamma 16\,\frac{1-z}{z^2}\,, \tag{1.9}$$

where

$$\delta_\gamma = 3f\langle e^4\rangle = 3\sum_i e_i^4\,, \tag{1.10}$$

the sum i runs over quarks of f flavors, and m_q is the quark mass. Because of the pointlike coupling of photon to quarks $\bar{W}_T^\gamma|_{\rm PM}$ does not scale, but grows logarithmically with q^2.

Recently QCD predictions for this process have been obtained in the leading order of asymptotic freedom by Llewellyn Smith[3] in the framework of perturbative QCD and Koller *et al.*[7,8] in the framework of the Altarelli-Parisi approach.[9] They found that the structure function $\bar{W}_T^\gamma$ maintains the nonscaling $\ln q^2$ behavior, but its shape changes substantially from the simple parton-model prediction.

The calculation of the next-to-leading-order contributions is important at least in two respects. It is important for perturbation theories to estimate how large the corrections to the leading term are. Secondly, it is known that Λ, the single free parameter of QCD, is not specified by a leading-logarithm calculation.[10,11] In order to determine Λ it is necessary to include the next-to-leading-order contributions.

In this paper we shall analyze direct photon production in e^+e^- collisions using the cut-vertex formalism developed by Mueller[12] and shall calculate the next-to-leading-order QCD corrections. It is crucial in the analysis to introduce the bare cut vertex for two photons in addition to the usual fermion and gluon cut vertices. The pointlike nature of photons is taken into account by inclusion of two-photon cut vertices. The situation is very similar to the case of the deep-inelastic scattering off a photon target where we must consider the twist-two photon operator in addition to the usual quark and gluon operators.[1]

In the next section we derive a formal expression for the moments of $\bar{W}_T^\gamma$ and $\bar{W}_L^\gamma$ in the framework of the cut-vertex formalism. We discuss in some detail the necessity of introducing the bare cut vertex for two photons. In Sec. III we present one-loop and two-loop anomalous dimensions of cut vertices. Using these anomalous dimensions we evaluate in Sec. IV the first three leading terms of $\bar{W}_T^\gamma$ moments. In Sec. V we evaluate the leading term of $\bar{W}_L^\gamma$ moments. Section VI is devoted to a brief summary of this paper and some comments on the backgrounds to the direct photon production.

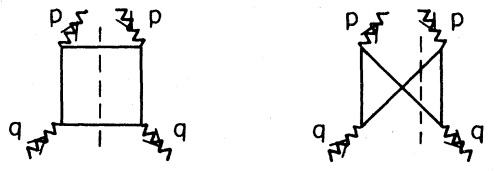

FIG. 2. Box diagrams for direct photon production.

II. CUT-VERTEX FORMALISM FOR DIRECT PHOTON PRODUCTION

In order to analyze hard-scattering processes we need to separate the dynamics into two regimes—that of large-distance effects which are connected with the formation of hadrons, and that of short-distance effects which are calculable in perturbative techniques. In deep-inelastic scattering, the light-cone expansion makes it possible to separate the large- and short-distance effects. This separation can be done even in semi-inclusive processes by using the cut-vertex formalism which has been developed by Mueller.[12,13]

In his pioneering work,[12] Mueller showed that the moments of the structure functions in single-particle inclusive e^+e^- annihilation factorize, for large q^2, into a singular function depending on the q^2 of the virtual photon, but completely independent of the particle produced, times a cut vertex which depends on the particle observed. He has introduced the bare cut vertices for two fermions, for two fermions with arbitrary number of gluons, and for gluons (see Fig. 5 below). But if the observed particle is a photon, we should consider an additional cut vertex—the cut vertex for two photons.

First consider the inclusive *hadron* production in e^+e^- collisions. For a given Feynman graph contributing to this process, we break up the graph into two parts which are connected by fermion and/or gluon propagators as shown in Fig. 3. Call the right-hand part of the graph τ and the left-hand part λ. Because of the composite nature of the hadron produced, we decompose the graph such that large momenta of order q^2 flow through τ, and not through λ. The addition subtraction

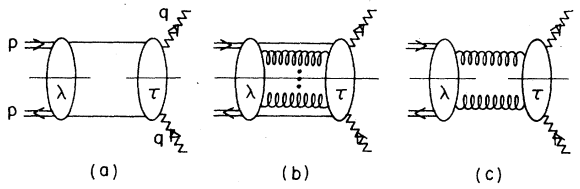

FIG. 3. Examples of decomposition of the amplitudes for inclusive hadron production in e^+e^- annihilation: (a) involving two fermions; (b) involving two fermions and many gluons; (c) involving two gluons. Double lines, solid lines, curly lines, and wavy lines represent hadron, quark, gluon, and photon, respectively.

procedure enables us to pick up the dominant term for large q^2 and to show that the moments of cross section are factored into a cut vertex times a singular function. (Details are discussed in Ref. 12.) Roughly speaking, after renormalization λ contributes to the *renormalized* fermion and gluon cut vertices, and the right-hand part τ contributes to the timelike coefficient functions.

Now consider the direct photon production in e^+e^- annihilation. The photon has two features: the photon interacts as though it were a vector meson with a transverse-momentum cutoff, but on the other hand it couples pointlike to quarks. If the photon has the first feature only, each contributing Feynman graph can be broken up into two parts just like those in Fig. 3, and the moments of the cross section (or the timelike photon structure functions) can be written in the factorized form, i.e., the fermion and gluon cut vertices times the timelike coefficient functions. However the second feature, the pointlike coupling of the photon to quarks, allows the different configuration of momentum flows from the ones in Fig. 3. Large momenta of order q^2 can flow all the way down to the real photon vertices, and the decomposition of the types shown in Fig. 3 is not adequate. We should include the contribution of each graph with this configuration of momentum flows, which is illustrated in Fig. 4. This latter contribution to the moments can also be written in a factorized form: this time, the *bare cut vertex for two photons* times a coefficient function. To lowest order in α the photon cut vertex needs no renormalization. Therefore, the *bare* photon cut vertex, when summed over the photon polarization and multiplied by an appropriate kinematical factor, turns out to be simply equal to one. The situation is exactly analogous to deep-inelastic scatterings off the photon target, in which we have introduced the photon operator, and the matrix element of the photon operator in a photon state is, to lowest order in α, equal to one.

Let us examine the contribution of Fig. 4 more closely. Call $M_{\alpha\beta,\mu\nu}(p,q)$ the renormalized amplitude for the four-photon vertex. For the moment we forget the polarization sum of the outgoing photon. Now consider the case where large momenta of order q^2 flow through the vertex and the decompositions of the types shown in Fig. 3 are not allowed. Then we should consider the vertex itself as a whole. Decompose $M_{\alpha\beta,\mu\nu}(p,q)$ into the different tensor structures as follows:

$$M_{\alpha\beta,\mu\nu}(p,q)=\sum_{i=L,2} t^i_{\alpha\beta,\mu\nu}(p,q)M^\gamma_i(p^2,p\cdot q,q^2)+\cdots, \tag{2.1}$$

where

$$t^L_{\alpha\beta,\mu\nu}(p,q)=2(g_{\mu\nu}q^2-q_\mu q_\nu)\times[g_{\alpha\beta}(p\cdot q)^2-(q_\alpha p_\beta+q_\beta p_\alpha)p\cdot q+q_\alpha q_\beta p^2]\frac{1}{(q^2)^3}, \tag{2.2}$$

$$t^2_{\alpha\beta,\mu\nu}(p,q)=\left(g_{\mu\nu}-\frac{q_\mu p_\nu+p_\mu q_\nu}{p\cdot q}+\frac{q^2}{(p\cdot q)^2}p_\mu p_\nu\right)\times[g_{\alpha\beta}(p\cdot q)^2-(q_\alpha p_\beta+q_\beta p_\alpha)p\cdot q+q_\alpha q_\beta p^2]\frac{1}{(q^2)^2}, \tag{2.3}$$

and the neglected terms in Eq. (2.1) do not contribute when we sum over the photon polarization in the final state. Setting $\mu=\nu=-$,[14] and for large q^2 and q_+ we obtain

$$t^L_{\alpha\beta,--}=-\frac{2q_-^2q_+^2}{(q^2)^3}[g_{\alpha\beta}p_-^2-p_-(g_{\alpha-}p_\beta+g_{\beta-}p_\alpha)+g_{\alpha-}g_{\beta-}p^2], \tag{2.4}$$

$$t^2_{\alpha\beta,--}=\frac{q_+^2}{(q^2)^2}[g_{\alpha\beta}p_-^2-p_-(g_{\alpha-}p_\beta+g_{\beta-}p_\alpha)+g_{\alpha-}g_{\beta-}p^2]. \tag{2.5}$$

When we sum up the polarization of the final photon, we obtain

$$-\sum_{\alpha,\beta}g^{\alpha\beta}M_{\alpha\beta,--}(p,q)=\frac{4q_-^2\nu^2}{(q^2)^3}M^\gamma_L(0,\nu,q^2)-\frac{2q_+^2p_-^2}{(q^2)^2}M^\gamma_2(0,\nu,q^2). \tag{2.6}$$

Taking the $(-,-)$ combination for $\overline{W}^\gamma_{\mu\nu}$ in Eq. (1.2) and comparing it with the result of Eq. (2.6), we find, for the contribution of graphs with the large-momentum-flow configurations shown in Fig. 4 to the photon structure functions

$$\overline{W}^\gamma_L(z,q^2)=z^2M^\gamma_L(0,z,q^2), \tag{2.7}$$

$$\nu\overline{W}^\gamma_2(z,q^2)=zM^\gamma_2(0,z,q^2). \tag{2.8}$$

The moments are then given as

$$\int_0^1 dz\, z^n\overline{W}^\gamma_L(z,q^2)=\int_0^1 dz\, z^{n+2}M^\gamma_L(0,z,q^2)=E^\gamma_{L,n}(q^2), \tag{2.9}$$

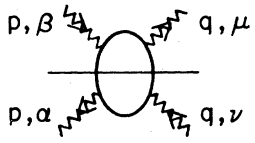

FIG. 4. The amplitude occurring in direct photon production, where large momenta of order q^2 flow through the blob.

$$\int_0^1 dz\, z^{n+1}\nu\overline{W}_2^\gamma(z,q^2)=\int_0^1 dz\, z^{n+2}M_2^\gamma(0,z,q^2)$$
$$=E_{2,n}^\gamma(q^2)\,. \tag{2.10}$$

The above equations can be rewritten in another form,

$$\int_0^1 dz\, z^n\overline{W}_L^\gamma(z,q^2)=v_n^\gamma(p^2)E_{L,n}^\gamma(q^2)\,, \tag{2.11}$$

$$\int_0^1 dz\, z^{n+1}\nu\overline{W}_2^\gamma(z,q^2)=v_n^\gamma(p^2)E_{2,n}^\gamma(q^2)\,, \tag{2.12}$$

where

$$v_n^\gamma(p^2)=1$$
$$=\sum_{\alpha,\beta} g^{\alpha\beta}\tfrac{1}{8}p_-^{n-1}\Gamma_{\alpha\beta,n}^\gamma(p)\,, \tag{2.13}$$

and

$$\Gamma_{\alpha\beta,n}^\gamma(p)=4[g_{\alpha\beta}p_-^{\,2}-p_-(g_{\alpha-}p_\beta+g_{\beta-}p_\alpha)$$
$$+g_{\alpha-}g_{\beta-}p^2](p_-)^{-n-1}\,. \tag{2.14}$$

The expression of Eq. (2.14) is exactly the same form as the two-gluon cut vertex [see Eq. (2.17) below], and we can call $\Gamma_{\alpha\beta,n}^\gamma(p)$ the bare cut vertex for two photons. It is illustrated in Fig. 5(a).

Now we list the other (timelike) bare cut vertices which we need for analysis of the direct photon production in e^+e^- annihilation. The flavor-singlet cut vertices for two fermions without and with one gluon are[12,13]

$$\text{Fig. 5(b):}\quad \Gamma_{\psi,n}^{ab}(p)=\gamma_-p_-^{-n}\delta_{ab}1\,,$$

$$\text{Fig. 5(c):}\quad \Gamma_{\psi,n}^{ai,b}(p,k)=\frac{g\gamma_-}{k_-}T_{ab}^i(p+k)_-^{-n}1\,,$$

$$\text{Fig. 5(d):}\quad \Gamma_{\psi,n}^{a,bi}(p,k)=-\frac{g\gamma_-}{k_-}T_{ab}^i p_-^{-n}1\,. \tag{2.15}$$

The indices a, b refer to a representation R of the color group SU(3) for fermions, g is the strong coupling constant of the theory, and 1 is then $f\times f$ unit matrix. These vertices obey the following Ward-Takahashi (WT) identities:

$$k_-\Gamma_{\psi,n}^{ai,b}(p,k)=gT_{ac}^i\Gamma_{\psi,n}^{cb}(p+k)\,,$$
$$k_-\Gamma_{\psi,n}^{a,bi}(p,k)=-g\Gamma_{\psi,n}^{ab}(p)T_{bb}^i\,. \tag{2.16}$$

We must add the cut vertices for two fermions with more gluons. Vertices with extra gluons become rather complicated, but their form is essentially fixed by the WT identities and the bare fermion cut vertices without gluons. Therefore we have not listed higher-order vertices.

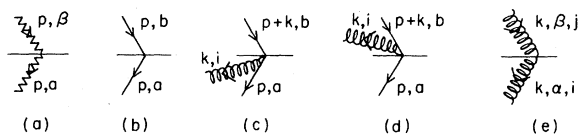

FIG. 5. Timelike cut vertices for direct photon production.

The formulas for the flavor-nonsinglet cut vertices for two fermions without and with gluons are the same as the singlet ones with the replacement of 1 by $(Q_{\rm ch}^2-\langle e^2\rangle 1)$, where $Q_{\rm ch}^2$ is the square of the $f\times f$ quark charge matrix, and $\langle e^2\rangle$ is the average quark charge squared.

The cut vertex for two gluons is given by Fig. 5(e),

$$\Gamma_{\alpha\beta,n}^{ij}(k)=4\delta_{ij}[\,g_{\alpha\beta}k_-^{\,2}-k_-(g_{\alpha-}k_\beta+g_{\beta-}k_\alpha)$$
$$+g_{\alpha-}g_{\beta-}k^2](k_-)^{-n-1}\,. \tag{2.17}$$

We need cut vertices for more gluons. The higher-order vertices are straightforward to construct with resort to the WT identities, but they are somewhat cumbersome. The three-gluon vertices, for example, are shown in Ref. 12.

With all these cut vertices at hand, we follow Mueller's cut vertex formalism which has been discussed in detail in Ref. 12. Then for large q^2 the moments of the timelike photon structure functions are given in a factorized form as follows:

$$\int_0^1 dz\, z^n\overline{W}_L^\gamma(z,q^2)=\sum_i v_n^i E_{L,n}^i\left(\frac{q^2}{\mu^2},g^2,\alpha\right), \tag{2.18}$$

$$\int_0^1 dz\, z^{n+1}\nu\overline{W}_2^\gamma(z,q^2)=\sum_i v_n^i E_{2,n}^i\left(\frac{q^2}{\mu^2},g^2,\alpha\right), \tag{2.19}$$

where the sum i runs over ψ, G, NS, and γ, and μ^2 is the subtraction scale at which the theory is renormalized. The q^2 dependence of the structure functions enters into the timelike coefficient functions $E_{L,n}^i$ and $E_{2,n}^i$. On the other hand, v_n^i does not depend on q^2, but is dependent on the particle observed. Especially we have $v_n^\gamma=1$ from Eq. (2.13). The hadronic feature of the photon is taken into account within v_n^ψ, v_n^G, and $v_n^{\rm NS}$.

The same cut vertices contribute to the moments of $\overline{W}_L^\gamma$ and $\nu\overline{W}_2^\gamma$. Therefore, from Eqs. (1.5) and (1.6) the moments of the transverse structure function $\overline{W}_T^\gamma$ are given with the same v_n^i as follows:

$$\int_0^1 dz\, z^n\overline{W}_T^\gamma(z,q^2)=\sum_i v_n^i E_{T,n}^i\left(\frac{q^2}{\mu^2},g^2,\alpha\right), \tag{2.20}$$

with $i=\psi$, G, NS, and γ. In what follows we work with the moments of $\overline{W}_T^\gamma$ and $\overline{W}_L^\gamma$.

The q^2 dependence of $E_{T,n}^i$ and $E_{L,n}^i$ in Eqs. (2.20) and (2.18) is governed by the same renormalization-group equation (RGE). If we describe the

coefficient function by the column vector

$$\vec{\mathbf{E}}_{k,n}\left(\frac{q^2}{\mu^2}, g^2, \alpha\right) = \begin{bmatrix} E^{\psi}_{k,n}\left(\frac{q^2}{\mu^2}, g^2, \alpha\right) \\ E^{G}_{k,n}\left(\frac{q^2}{\mu^2}, g^2, \alpha\right) \\ E^{\mathrm{NS}}_{k,n}\left(\frac{q^2}{\mu^2}, g^2, \alpha\right) \\ E^{\gamma}_{k,n}\left(\frac{q^2}{\mu^2}, g^2, \alpha\right) \end{bmatrix}, \quad k = T, L, \tag{2.21}$$

then $\vec{\mathbf{E}}_{k,n}$ obeys the lowest order in α, the following RGE,

$$\left(\mu\frac{\partial}{\partial\mu} + \beta(g)\frac{\partial}{\partial g}\right)\vec{\mathbf{E}}_{k,n}\left(\frac{q^2}{\mu^2}, g^2, \alpha\right) = \bar{\gamma}_n(g^2, \alpha)\vec{\mathbf{E}}_{k,n}\left(\frac{q^2}{\mu^2}, g^2, \alpha\right), \tag{2.22}$$

where $\beta(g)$ is the well-known renormalization function and $\bar{\gamma}_n(g^2, \alpha)$ is the anomalous-dimension matrix of the cut vertices. To lowest order in α this matrix has the form

$$\bar{\gamma}_n(g^2, \alpha) = \begin{bmatrix} \bar{\gamma}^n_{\psi\psi}(g^2) & \bar{\gamma}^n_{G\psi}(g^2) & 0 & 0 \\ \bar{\gamma}^n_{\psi G}(g^2) & \bar{\gamma}^n_{GG}(g^2) & 0 & 0 \\ 0 & 0 & \bar{\gamma}^n_{\mathrm{NS}}(g^2) & 0 \\ K^n_{\psi}(g^2, \alpha) & K^n_{G}(g^2, \alpha) & K^n_{\mathrm{NS}}(g^2, \alpha) & 0 \end{bmatrix}. \tag{2.23}$$

The solution of the RGE (2.22) is given by

$$\vec{\mathbf{E}}_{k,n}\left(\frac{q^2}{\mu^2}, g^2, \alpha\right) = \left[T_g \exp\left(\int_{\bar{g}}^{g} dg' \frac{\bar{\gamma}_n(g'^2, \alpha)}{\beta(g')}\right)\right]\vec{\mathbf{E}}_{k,n}(1, \bar{g}^2, \alpha). \tag{2.24}$$

Here T_g represents T ordering, and $\bar{g}^2$ is the running coupling constant of the strong interaction which satisfies the following equation:

$$\frac{d}{dt}\bar{g}(t, g) = \beta(\bar{g}), \quad \bar{g}(0, g) = g \tag{2.25}$$

with $t = (\frac{1}{2})\ln(q^2/\mu^2)$.

We observe that the RGE (2.22), the anomalous-dimension matrix in (2.23), and the solution (2.24) of the RGE have exactly the same forms as those we had in the deep-inelastic scattering off the photon target.[1,2] In the latter case Bardeen and Buras have explained the solution of the RGE in detail and have calculated the next-to-leading-order contributions in Ref. 2. Therefore we can follow the same procedures as they did to evaluate the first few leading terms for the moments of the timelike photon structure functions $\overline{W}^{\gamma}_T$ and $\overline{W}^{\gamma}_L$. Moreover we can adopt the formulas in Secs. II, III, and V of Ref. 2 with the replacement of the anomalous dimensions of operators by those of cut vertices, and of the coefficient functions $C^i_n(1, \bar{g}^2, \alpha)$ by $E^i_{k,n}(1, \bar{g}^2, \alpha)$.

III. ANOMALOUS DIMENSIONS OF CUT VERTICES

For the evaluation of the T-ordered exponential in Eq. (2.24) we expand $\bar{\gamma}_n(g^2, \alpha)$ and $\beta(g)$ in powers of g as follows:

$$\bar{\gamma}^n_{ij}(g^2) = \bar{\gamma}^{0,n}_{ij}\frac{g^2}{16\pi^2} + \bar{\gamma}^{1,n}_{ij}\frac{g^4}{(16\pi^2)^2} + \cdots, \quad i, j = \psi, G, \tag{3.1}$$

$$\bar{\gamma}^n_{\mathrm{NS}}(g^2) = \bar{\gamma}^{0,n}_{\mathrm{NS}}\frac{g^2}{16\pi^2} + \bar{\gamma}^{1,n}_{\mathrm{NS}}\frac{g^4}{(16\pi^2)^2} + \cdots, \tag{3.2}$$

$$K^n_i(g^2, \alpha) = -\bar{K}^{0,n}_i\frac{e^2}{16\pi^2} - \bar{K}^{1,n}_i\frac{e^2g^2}{(16\pi^2)^2} + \cdots, \quad i = \psi, G, \mathrm{NS}, \tag{3.3}$$

and

$$\beta(g) = -\beta_0\frac{g^3}{16\pi^2} - \beta_1\frac{g^5}{(16\pi^2)^2}, \tag{3.4}$$

with[15]

$$\beta_0 = 11 - \tfrac{2}{3}f, \quad \beta_1 = 102 - \tfrac{38}{3}f.$$

We also expand $\bar{g}^2(q^2)$, the solution of Eq. (2.25) with $\beta(g)$ given by (3.4), in powers of $\bar{g}_0{}^2(q^2)$, the effective coupling constant calculated in the one-loop approximation, with the result

$$\bar{g}^2(q^2) = \bar{g}_0{}^2(q^2) - \frac{\beta_1}{\beta_0}\frac{\bar{g}_0{}^4(q^2)}{16\pi^2}\ln\ln\frac{q^2}{\Lambda^2} + O(\bar{g}_0{}^6), \tag{3.5}$$

where

$$\bar{g}_0{}^2(q^2) = \frac{16\pi^2}{\beta_0\ln(q^2/\Lambda^2)}. \tag{3.6}$$

Now we list the one-loop and the two-loop anomalous dimensions of cut vertices.

A. One-loop anomalous dimensions

For the hadronic sector the one-loop anomalous dimensions have been calculated in Refs. 12 and 16,

$$\bar{\gamma}^{0,n}_{\psi\psi} = \bar{\gamma}^{0,n}_{\mathrm{NS}} = \frac{8}{3}\left[-3 - \frac{2}{n(n+1)} + 4S_1(n)\right], \tag{3.7}$$

$$\bar{\gamma}^{0,n}_{\psi G} = -4f\frac{n^2+n+2}{(n-1)n(n+1)}, \tag{3.8}$$

$$\bar{\gamma}^{0,n}_{G\psi} = -\frac{16}{3}\frac{n^2+n+2}{n(n+1)(n+2)}, \tag{3.9}$$

$$\bar{\gamma}_{GG}^{0,n}=6\left[-\frac{11}{3}-\frac{4}{(n-1)n}-\frac{4}{(n+1)(n+2)}+4S_1(n)\right]+\tfrac{4}{3}f, \tag{3.10}$$

where

$$S_1(n)=\sum_{j=1}^{n}\frac{1}{j}. \tag{3.11}$$

The anomalous dimensions $\bar{K}_{\psi}^{0,n}$ and $\bar{K}_{\mathrm{NS}}^{0,n}$ are obtained from (3.8) by replacing the group-theory factor $f/2[=T(R)]$ by the relevant charge factors, with the result

$$\bar{K}_{\psi}^{0,n}=8\frac{n^2+n+2}{(n-1)n(n+1)}3f\langle e^2\rangle, \tag{3.12}$$

$$\bar{K}_{\mathrm{NS}}^{0,n}=8\frac{n^2+n+2}{(n-1)n(n+1)}3f(\langle e^4\rangle-\langle e^2\rangle^2). \tag{3.13}$$

Also we have in one-loop approximations

$$\bar{K}_{G}^{0,n}=0. \tag{3.14}$$

B. Two-loop anomalous dimenions

For the pure hadronic sector the two-loop anomalous dimensions of cut vertices can be obtained by taking moments of the next-to-leading parton decay probability functions, i.e., a generalization of the Altarelli-Parisi probabilities[9] to two-loop level. Recently three groups have calculated the probability functions in two-loop approximations.[17-19] The $\bar{g}^2$ corrections to $E_{k,n}^{i}(1,\bar{g}^2,\alpha)$ in Eq. (2.24) can be obtained by taking moments of the one-loop corrections to the "short-distance cross sections" (SDCS) which have been calculated by Altarelli *et al.*[20] and later by the authors of Refs. 17 and 18.

It is well known[21] that in deep-inelastic scatterings the anomalous dimensions of the relevant operators in the two-loop and the $\bar{g}^2$ corrections to the coefficient functions $C_n^i(1,\bar{g}^2)$ are renormalization-prescription dependent. Only when both are calculated in the same renormalization scheme and are put into the physical quantities does their renormalization-prescription dependence cancel out. The same thing happens in the case of the single-particle inclusive e^+e^- annihilation. In our analysis of $\bar{W}_T^{\gamma}$, therefore, we should use the two-loop anomalous dimensions of cut vertices and the $\bar{g}^2$ corrections to the coefficient functions $E_{T,n}^{i}(1,\bar{g}^2,\alpha)$ which are calculated in the same renormalization scheme. [In the case of $\bar{W}_L$, we do not need the two-loop anomalous dimensions of cut vertices and the $\bar{g}^2$ corrections to $E_{L,n}^{i}(1,\bar{g}^2,\alpha)$ are renormalization-prescription independent. See Sec. V.]

So far, the calculations of the two-loop probability functions by three groups[17-19] and of the $\bar{g}^2$ corrections to the SDCS by four groups[17-20] have been done in the same 't Hooft minimal-subtraction scheme.[22] However there still remains a subtle scheme dependence. As shown clearly in Ref. 19 a different convention to define the SDCS gives a different result for the two-loop probability functions, although the physical quantities are scheme independent. In what follows we shall adopt the results of Ref. 17 for the next-to-leading probability functions, and of Ref. 20 for the SDCS, since the authors of both references have used the same convention to define the SDCS.

The two-loop anomalous dimensions of cut vertices $\bar{\gamma}_{ij}^{1,n}$ in the singlet sector are obtained by taking the moments of the two-loop parton decay probability functions $P_{AB}^{(1,T)}(x)$ given in the second paper of Ref. 17. Before presenting the results, we need several definitions:

$$C_F=\tfrac{4}{3},\quad C_G=3,\quad T(R)=\frac{f}{2},$$

$$S_2(n)=\sum_{j=1}^{n}\frac{1}{j^2},$$

$$S_2'\left(\frac{n}{2}\right)=\sum_{j=1}^{n/2}\frac{1}{j^2}\quad\text{for even } n,$$

$$S_3'\left(\frac{n}{2}\right)=\sum_{j=1}^{n/2}\frac{1}{j^3}\quad\text{for even } n,$$

$$\tilde{S}(n)=\sum_{k=1}^{n}\frac{(-1)^k}{k^2}\sum_{j=1}^{k}\frac{1}{j}. \tag{3.15}$$

We obtain for $n\geq 2$

$$\bar{\gamma}_{\psi\psi}^{1,n}=-8\int_0^1 P_{FF}^{(1,T)}(x)\,x^{n-1}dx$$
$$=-8[C_F{}^2A_{\psi\psi}(n)+C_FC_GB_{\psi\psi}(n)+C_FT(R)D_{\psi\psi}(n)], \tag{3.16}$$

with

$$A_{\psi\psi}(n)=\left[2S_1(n)-\frac{1}{n(n+1)}\right]\left[-6S_2(n)+2S_2'\left(\frac{n}{2}\right)+\frac{2}{3}\pi^2\right]-8\tilde{S}(n)+S_3'\left(\frac{n}{2}\right)+3S_2(n)+\left[\frac{2}{n^2}-\frac{2}{(n+1)^2}\right]S_1(n)$$
$$-\frac{1}{n^3}-\frac{1}{(n+1)^3}+\frac{1}{(n+1)^2}-\frac{1}{n}+\frac{1}{n+1}+\frac{3}{8}-\pi^2, \tag{3.17}$$

$$B_{\psi\psi}(n)=\left[2S_1(n)-\frac{1}{n(n+1)}\right]\left[2S_2(n)-S_2'\left(\frac{n}{2}\right)-\frac{67}{18}\right]+4\tilde{S}(n)-\tfrac{1}{2}S_3'\left(\frac{n}{2}\right)+\frac{11}{3}S_2(n)$$
$$-\frac{11}{6}\frac{1}{n^2}+\frac{11}{6}\frac{1}{(n+1)^2}+\frac{14}{3}\frac{1}{n}-\frac{14}{3}\frac{1}{n+1}+\frac{17}{24}, \tag{3.18}$$

$$D_{\psi\psi}(n)=\frac{10}{9}\left[2S_1(n)-\frac{1}{n(n+1)}\right]-\frac{4}{3}S_2(n)+\frac{4}{n^3}+\frac{4}{(n+1)^3}+\frac{32}{3}\frac{1}{n^2}+\frac{52}{3}\frac{1}{(n+1)^2}+\frac{16}{3}\frac{1}{(n+2)^2}$$
$$-\frac{52}{3}\frac{1}{n}+\frac{28}{3}\frac{1}{n+1}+\frac{112}{9}\frac{1}{n+2}-\frac{40}{9}\frac{1}{n-1}-\frac{1}{6}, \tag{3.19}$$

and[23]

$$\bar{\gamma}_{\psi G}^{1,n}=-8\frac{2T(R)}{C_F}\int_0^1 P_{FG}^{(1,T)}(x)x^{n-1}dx=-16[C_F T(R)D_{\psi G}(n)+C_G T(R)H_{\psi G}(n)], \tag{3.20}$$

with

$$D_{\psi G}(n)=\frac{n^2+n+2}{(n-1)n(n+1)}\left[S_1^2(n)-3S_2(n)-\tfrac{2}{3}\pi^2\right]+S_1(n)\left[\frac{8}{(n-1)^2}-\frac{8}{n^2}+\frac{6}{(n+1)^2}-\frac{4}{n-1}+\frac{4}{n}-\frac{2}{n+1}\right]$$
$$+\frac{16}{n-1}-\frac{33}{2}\frac{1}{n}+\frac{9}{2}\frac{1}{n+1}-\frac{8}{(n-1)^2}-\frac{5}{2}\frac{1}{(n+1)^2}+\frac{2}{n^3}+\frac{1}{(n+1)^3}, \tag{3.21}$$

$$H_{\psi G}(n)=\frac{n^2+n+2}{(n-1)n(n+1)}\left[-S_1^2(n)+7S_2(n)-S_2'\left(\frac{n}{2}\right)\right]+S_1(n)\left[-\frac{4}{(n-1)^2}+\frac{4}{n^2}-\frac{4}{(n+1)^2}+\frac{4}{n-1}-\frac{4}{n}+\frac{2}{n+1}\right]$$
$$-\frac{8}{(n-1)^3}-\frac{4}{n^3}-\frac{2}{(n+1)^3}+\frac{10}{(n-1)^2}-\frac{7}{(n+1)^2}-\frac{8}{3}\frac{1}{(n+2)^2}-\frac{91}{9}\frac{1}{n-1}+\frac{17}{n}-\frac{1}{n+1}-\frac{44}{9}\frac{1}{n+2}, \tag{3.22}$$

and

$$\bar{\gamma}_{G\psi}^{1,n}=-8\frac{C_F}{2T(R)}\int_0^1 P_{GF}^{(1,T)}(x)x^{n-1}dx=-4[C_F{}^2A_{G\psi}(n)+C_F C_G B_{G\psi}(n)+C_F T(R)D_{G\psi}(n)], \tag{3.23}$$

with

$$A_{G\psi}(n)=\frac{n^2+n+2}{n(n+1)(n+2)}[-2S_1{}^2(n)+10S_2(n)]$$
$$+S_1(n)\left[-\frac{4}{n^2}+\frac{16}{(n+1)^2}-\frac{16}{(n+2)^2}+\frac{6}{n}-\frac{12}{n+1}+\frac{12}{n+2}\right]$$
$$-\frac{2}{n^3}-\frac{4}{(n+1)^3}+\frac{5}{n^2}+\frac{8}{(n+1)^2}+\frac{16}{(n+2)^2}-\frac{12}{n}-\frac{5}{n+1}+\frac{8}{n+2}, \tag{3.24}$$

$$B_{G\psi}(n)=\frac{n^2+n+2}{n(n+1)(n+2)}\left[2S_1{}^2(n)-2S_2(n)-2S_2'\left(\frac{n}{2}\right)-\frac{4}{3}\pi^2\right]$$
$$+S_1(n)\left[\frac{8}{n^2}-\frac{24}{(n+1)^2}+\frac{24}{(n+2)^2}-\frac{22}{3}\frac{1}{n}+\frac{44}{3}\frac{1}{n+1}-\frac{44}{3}\frac{1}{n+2}\right]$$
$$+\frac{4}{n^3}+\frac{8}{(n+1)^3}+\frac{8}{3}\frac{1}{n^2}+\frac{88}{3}\frac{1}{(n+1)^2}-\frac{28}{(n+2)^2}-\frac{40}{9}\frac{1}{n-1}+\frac{26}{9}\frac{1}{n}-\frac{34}{9}\frac{1}{n+1}+\frac{200}{9}\frac{1}{n+2}, \tag{3.25}$$

$$D_{G\psi}(n)=\frac{n^2+n+2}{n(n+1)(n+2)}\left[\frac{8}{3}S_1(n)-\frac{40}{9}\right]+\frac{8}{3}\left[\frac{1}{n^2}-\frac{4}{(n+1)^2}+\frac{4}{(n+2)^2}\right], \tag{3.26}$$

and

$$\bar{\gamma}_{GG}^{1,n}=-8\int_0^1 P_{GG}^{(1,T)}(x)x^{n-1}dx=-8\{C_F T(R)D_{GG}(n)+C_G T(R)H_{GG}(n)+C_G{}^2L_{GG}(n)\}, \tag{3.27}$$

with

$$D_{GG}(n)=\frac{4}{n^3}+\frac{4}{(n+1)^3}-\frac{16}{3}\frac{1}{(n-1)^2}-\frac{10}{n^2}-\frac{14}{(n+1)^2}-\frac{16}{3}\frac{1}{(n+2)^2}+\frac{92}{9}\frac{1}{n-1}-\frac{4}{n}+\frac{12}{n+1}-\frac{164}{9}\frac{1}{n+2}-1, \quad (3.28)$$

$$H_{GG}(n)=-\tfrac{8}{3}S_2(n)+\tfrac{20}{9}S_1(n)+\frac{8}{3}\frac{1}{(n-1)^2}-\frac{4}{3}\frac{1}{n^2}+\frac{4}{(n+1)^2}-\frac{8}{3}\frac{1}{(n+2)^2}-\frac{46}{9}\frac{1}{n-1}$$
$$+\frac{38}{9}\frac{1}{n}-\frac{38}{9}\frac{1}{n+1}+\frac{46}{9}\frac{1}{n+2}-\frac{4}{3}+\frac{4}{9}\pi^2, \quad (3.29)$$

$$L_{GG}(n)=-4\tilde{S}(n)+\tfrac{22}{3}S_2(n)+\tfrac{1}{2}S_3'\left(\frac{n}{2}\right)+\left[S_1(n)-\frac{1}{n-1}+\frac{1}{n}-\frac{1}{n+1}+\frac{1}{n+2}\right]\left[-8S_2(n)+2S_2'\left(\frac{n}{2}\right)+\frac{4}{3}\pi^2\right]$$
$$+S_1(n)\left[\frac{4}{(n-1)^2}-\frac{4}{n^2}+\frac{4}{(n+1)^2}-\frac{4}{(n+2)^2}-\frac{67}{9}\right]-\frac{8}{(n-1)^3}-\frac{4}{n^3}-\frac{4}{(n+1)^3}+\frac{10}{3}\frac{1}{(n-1)^2}$$
$$+\frac{11}{3}\frac{1}{n^2}-\frac{7}{(n+1)^2}+\frac{34}{3}\frac{1}{(n+2)^2}+\frac{4}{n-1}+\frac{37}{18}\frac{1}{n}-\frac{37}{18}\frac{1}{n+1}-\frac{4}{n+2}+\frac{8}{3}-\frac{11}{9}\pi^2. \quad (3.30)$$

The factors $2T(R)/C_F$ and $C_F/2T(R)$ have been inserted in Eqs. (3.20) and (3.23), respectively, for the following reason: the authors of Ref. 17 have calculated $P_{FG}^{(1,T)}(x)$ by summing over gluons but not over quark flavors, and $P_{GF}^{(1,T)}(x)$ by summing vice versa. However, in order to obtain $\bar{\gamma}_{\psi G}^{1,n}$ we should sum over quark flavors but not over gluons. For $\bar{\gamma}_{G\psi}^{1,n}$ we should sum vice versa. In fact we can obtain the correct one-loop nondiagonal anomalous dimension $\bar{\gamma}_{\psi G}^{0,n}$ and $\bar{\gamma}_{G\psi}^{0,n}$ in Eqs. (3.8) and (3.9) by taking moments of the one-loop nondiagonal probability functions $P_{FG}^{(0,T)}(x)$ and $P_{GF}^{(0,T)}(x)$ given in Ref. 17, and multiplying them by $2T(R)/C_F$ and $C_F/2T(R)$, respectively.

The two-loop anomalous dimension of the nonsinglet cut vertex has been calculated first in the first paper of Ref. 17 with the result for even $n\geq 2$

$$\bar{\gamma}_{\rm NS}^{1,n}=\gamma_{\rm NS}^{1,n}-16{C_F}^2\left[-2S_1(n)+\frac{1}{n(n+1)}+\frac{3}{2}\right]\left[2S_2(n)-\frac{2n+1}{n^2(n+1)^2}-\frac{\pi^2}{3}\right], \quad (3.31)$$

where

$$\gamma_{\rm NS}^{1,n}=({C_F}^2-\tfrac{1}{2}C_FC_G)\left\{16S_1(n)\frac{2n+1}{n^2(n+1)^2}+16\left[2S_1(n)-\frac{1}{n(n+1)}\right]\left[S_2(n)-S_2'\left(\frac{n}{2}\right)\right]+64\tilde{S}(n)+24S_2(n)\right.$$
$$\left.-3-8S_3'\left(\frac{n}{2}\right)-8\frac{3n^3+n^2-1}{n^3(n+1)^3}-16\frac{2n^2+2n+1}{n^3(n+1)^3}\right\}$$
$$+C_FC_G\left\{S_1(n)\left[\frac{536}{9}+8\frac{2n+1}{n^2(n+1)^2}\right]-16S_1(n)S_2(n)+S_2(n)\left[-\frac{52}{3}+\frac{8}{n(n+1)}\right]-\frac{43}{6}\right.$$
$$\left.-4\frac{151n^4+263n^3+97n^2+3n+9}{9n^3(n+1)^3}\right\}$$
$$+C_FT(R)\left[-\frac{160}{9}S_1(n)+\frac{32}{3}S_2(n)+\frac{4}{3}+16\frac{11n^2+5n-3}{9n^2(n+1)^2}\right] \quad (3.32)$$

is the two-loop anomalous dimension of the nonsinglet operator which appears in the deep-inelastic scatterings.[21,24]

The two-loop anomalous dimensions $\bar{K}_{\psi}^{1,n}$, $\bar{K}_{\rm NS}^{1,n}$, and $\bar{K}_{G}^{1,n}$ can be obtained from $\bar{\gamma}_{\psi G}^{1,n}$ and $\bar{\gamma}_{GG}^{1,n}$ by picking the terms proportional to $C_FT(R)$, replacing the factor $T(R)(=f/2)$ by the relevant charge factors, with the result

$$\bar{K}_{\psi}^{1,n}=16C_FD_{\psi G}(n)3f\langle e^2\rangle, \quad (3.33)$$

$$\bar{K}_{\rm NS}^{1,n}=16C_FD_{\psi G}(n)3f(\langle e^4\rangle-\langle e^2\rangle^2), \quad (3.34)$$

$$\bar{K}_{G}^{1,n}=8C_FD_{GG}(n)3f\langle e^2\rangle. \quad (3.35)$$

We give numerical values for the two-loop anomalous dimensions of timelike cut vertices in Table I. It is interesting to compare these values with those for the two-loop anomalous dimensions of relevant operators in deep-inelastic scattering off a photon target, which are listed in Tables I and II of Ref. 2. Note large negative values of $\bar{K}_{\psi}^{1,n}$ and $\bar{K}_{\rm NS}^{1,n}$ for the first several n's. They result from a term $-(\frac{2}{3})\pi^2$ in the expression for $D_{\psi G}(n)$ in Eq. (3.21). Also π^2 terms appear in the expressions of two-loop anomalous dimensions of timelike cut vertices. They are due to the analytic continuation from a spacelike region to a timelike region.

For large n we obtain the following asymptotic forms for $\bar{\gamma}_{ij}^{1,n}(i,j=\psi,G)$ and $\bar{\gamma}_{\rm NS}^{1,n}$:

$$\bar{\gamma}_{\psi\psi}^{1,n}\underset{n\to\infty}{\sim}\bar{\gamma}_{\rm NS}^{1,n}\underset{n\to\infty}{\sim}[(\tfrac{536}{9}-\tfrac{8}{3}\pi^2)C_FC_G-\tfrac{160}{9}C_FT(R)]\ln n,$$

TABLE I. Coefficients of $g^4/(16\pi^2)^2$ in the anomalous dimensions $\bar{\gamma}^n_{\rm NS}$, $\bar{\gamma}^n_{\psi\psi}$, $\bar{\gamma}^n_{\psi G}$, $\bar{\gamma}^n_{G\psi}$, and $\bar{\gamma}^n_{GG}$, and coefficients of $e^2g^2/(16\pi^2)^2$ in the anomalous dimensions $\bar{K}^n_\psi$, $\bar{K}^n_{\rm NS}$, and $\bar{K}^n_G$ for $f=4$.

n	$\bar{\gamma}^{1,n}_{\rm NS}$	$\bar{\gamma}^{1,n}_{\psi\psi}$	$\bar{\gamma}^{1,n}_{\psi G}$	$\bar{\gamma}^{1,n}_{G\psi}$	$\bar{\gamma}^{1,n}_{GG}$	$\bar{K}^{1,n}_\psi$	$\bar{K}^{1,n}_{\rm NS}$	$\bar{K}^{1,n}_G$
2	36.15	61.43	−184.3	23.43	−70.30	−249.9	−24.99	−85.60
4	85.52	90.21	−191.8	7.169	−61.80	−102.8	−10.28	−37.72
6	116.8	118.9	−112.8	3.536	33.50	−57.71	−5.771	−36.11
8	139.8	141.0	−76.60	1.646	97.54	−36.46	−3.646	−35.79
10	158.0	158.8	−56.29	0.494	146.0	−24.33	−2.433	−35.68
12	173.1	173.7	−43.41	−0.266	185.0	−16.61	−1.661	−35.63
14	186.0	186.4	−34.58	−0.794	217.8	−11.34	−1.134	−35.60
16	197.2	197.5	−28.19	−1.172	246.0	−7.56	−0.756	−35.59
18	207.2	207.4	−23.38	−1.451	270.7	−4.75	−0.475	−35.58
20	216.1	216.3	−19.64	−1.660	292.8	−2.60	−0.260	−35.57

$$\bar{\gamma}^{1,n}_{\psi G} \underset{n\to\infty}{\sim} -16(C_F - C_G)T(R)\frac{\ln^2 n}{n},$$

$$\bar{\gamma}^{1,n}_{G} \underset{n\to\infty}{\sim} -8(C_G - C_F)C_F\frac{\ln^2 n}{n},$$

$$\bar{\gamma}^{1,n}_{GG} \underset{n\to\infty}{\sim} \left[\left(\tfrac{539}{9} - \tfrac{8}{3}\pi^2\right)C_G{}^2 - \tfrac{160}{9}C_G T(R)\right]\ln n. \quad (3.36)$$

As was expected, $\bar{\gamma}^{1,n}_{ij}$ and $\bar{\gamma}^{1,n}_{\rm NS}$ have the same asymptotic behaviors as the spacelike counterparts.[24] Also $\bar{K}^{1,n}_\psi$ and $\bar{K}^{1,n}_{\rm NS}$ behave as $(1/n)\ln^2 n$, and $\bar{K}^{1,n}_G$ becomes $O(1)$ for large n.

IV. TRANSVERSE PHOTON STRUCTURE FUNCTION $\bar{W}^\gamma_T$

First we expand the coefficient functions $\vec{E}_{T,n}(1,\bar{g}^2,\alpha)$ in powers of $\bar{g}^2$ up to one-loop corrections as follows:

$$E^i_{T,n}(1,\bar{g}^2,\alpha) = \begin{cases} e^2\delta_\psi\left(1+\dfrac{\bar{g}^2}{16\pi^2}\bar{B}^n_{\psi,T}\right), & i=\psi, \quad (4.1)\\ e^2\delta_\psi\dfrac{\bar{g}^2}{16\pi^2}\bar{B}^n_{G,T}, & i=G, \quad (4.2)\\ e^2\delta_{\rm NS}\left(1+\dfrac{\bar{g}^2}{16\pi^2}\bar{B}^n_{{\rm NS},T}\right), & i={\rm NS}, \quad (4.3)\\ \dfrac{e^4}{16\pi^2}\delta_\gamma\bar{B}^n_{\gamma,T}, & i=\gamma, \quad (4.4)\end{cases}$$

where

$$\delta_\psi = \langle e^2\rangle = \sum_i e_i^2/f, \quad (4.5)$$

$$\delta_{\rm NS} = 1, \quad (4.6)$$

and δ_γ is given in Eq. (1.10). The $\bar{g}^2$ corrections to $E^i_{T,n}(1,\bar{g}^2,\alpha)$ with $i=\psi$, G, and NS are obtained by taking moments of the one-loop "short-distance cross sections" $d_q(z)$ and $d_G(z)$ given in Eqs. (64) and (65) of Ref. 20. They are

$$\bar{B}^n_{\psi,T} = \bar{B}^n_{{\rm NS},T} = \frac{4}{3}\left[10S_2(n) + 2S_1{}^2(n) + \left(3 - \frac{2}{n(n+1)}\right)S_1(n) - \frac{3}{n+1} - \frac{4}{n^2} + \frac{6}{(n+1)^2} - 9\right], \quad (4.7)$$

$$\bar{B}^n_{G,T} = 2f\left[-\frac{n^2+n+2}{(n-1)n(n+1)}S_1(n) - \frac{4}{(n-1)^2} + \frac{4}{n^2} - \frac{3}{(n+1)^2}\right]. \quad (4.8)$$

In Eq. (4.8) we have changed factor $\frac{4}{3}$ in Eq. (65) of Ref. 20 to $2f\,[=4T(R)]$ to match our definition of the coefficient functions. Also in Eqs. (4.7) and (4.8) we have discarded the terms proportional to $\ln(4\pi-\gamma_E)$, since it is possible to absorb them through a redefinition of the scale parameter Λ [modified minimal-subtraction ($\overline{\rm MS}$) scheme].[2,11]

$\bar{B}^n_{\gamma,T}$ is obtained from $\bar{B}^n_{G,T}$ by removing the group factor $T(R)$ and is given as

$$\bar{B}^n_{\gamma,T} = \frac{2}{f}\bar{B}^n_{G,T}. \quad (4.9)$$

With all information needed, we now follow the same procedures as Bardeen and Buras did in Ref. 2 to solve the RGE (2.24) for $\bar{W}^\gamma_T$. We obtain the QCD prediction for the moments of $\bar{W}^\gamma_T$, which is given in the following form:

$$\int_0^1 dz\, z^n \bar{W}^\gamma_T(z,q^2) = \alpha^2\left(\bar{a}_n\ln\frac{q^2}{\Lambda^2} + \bar{a}'_n\ln\ln\frac{q^2}{\Lambda^2} + \bar{b}_n\right). \quad (4.10)$$

The parameters $\bar{a}_n$, $\bar{a}'_n$, and $\bar{b}_n$ have the same expressions as a_n, $\bar{a}_n$, and b_n in Eqs. (3.23)–(3.25) of Ref. 2 except that all the anomalous dimensions and one-loop corrections to the coefficient functions are replaced by the timelike counter-

parts. They are given as follows:

$$\bar{a}_n=\frac{1}{2}\left[\frac{\bar{K}_\psi^{0,n}\delta_\psi}{\bar{d}_n}\left(1+\frac{\bar{\gamma}_{GG}^{0,n}}{2\beta_0}\right)+\frac{\bar{K}_{\rm NS}^{0,n}\delta_{\rm NS}}{1+\bar{\gamma}_{\rm NS}^{0,n}/2\beta_0}\right], \quad (4.11)$$

$$\bar{a}_n'=\frac{\beta_1}{\beta_0^2}\bar{a}_n, \quad n>2 \quad (4.12)$$

and

$$\bar{b}_n=\frac{\bar{K}_\psi^{1,n}\delta_\psi\bar{\gamma}_{GG}^{0,n}}{\bar{\lambda}_+^n\bar{\lambda}_-^n}-\frac{\bar{K}_G^{1,n}\delta_\psi\bar{\gamma}_{\psi G}^{0,n}}{\bar{\lambda}_+^n\bar{\lambda}_-^n}+\frac{\bar{K}_{\rm NS}^{1,n}\delta_{\rm NS}}{\bar{\gamma}_{\rm NS}^{0,n}}$$
$$+\frac{1}{2\beta_0}(\bar{K}_\psi^{0,n}\delta_\psi\bar{R}_{\psi,T}^n+\bar{K}_{\rm NS}^{0,n}\delta_{\rm NS}\bar{R}_{{\rm NS},T}^n)$$
$$+\bar{B}_{\gamma,T}^n\delta_\gamma, \quad n>2. \quad (4.13)$$

Here we have defined

$$\bar{\lambda}_\pm^n=\tfrac{1}{2}\{\bar{\gamma}_{\psi\psi}^{0,n}+\bar{\gamma}_{GG}^{0,n}\pm[(\bar{\gamma}_{\psi\psi}^{0,n}-\bar{\gamma}_{GG}^{0,n})^2+4\bar{\gamma}_{\psi G}^{0,n}\bar{\gamma}_{G\psi}^{0,n}]^{1/2}\}, \quad (4.14)$$

$$\bar{d}_n=\left(1+\frac{\bar{\lambda}_-^n}{2\beta_0}\right)\left(1+\frac{\bar{\lambda}_+^n}{2\beta_0}\right), \quad (4.15)$$

$$\bar{R}_{\psi,T}^n=\frac{\bar{B}_{\psi,T}^n}{\bar{d}_n}\left(1+\frac{\bar{\gamma}_{GG}^{0,n}}{2\beta_0}\right)-\frac{\bar{B}_{G,T}^n}{\bar{d}_n}\frac{\bar{\gamma}_{G\psi}^{0,n}}{2\beta_0}+\frac{\bar{\Delta}_n}{\bar{d}_n\bar{\lambda}_+^n\bar{\lambda}_-^n}-\frac{\beta_1}{\beta_0}\frac{(\bar{\gamma}_{GG}^{0,n})^2+2\beta_0\bar{\gamma}_{GG}^{0,n}+\bar{\gamma}_{\psi G}^{0,n}\bar{\gamma}_{G\psi}^{0,n}}{\bar{d}_n\bar{\lambda}_+^n\bar{\lambda}_-^n}, \quad (4.16)$$

$$\bar{R}_{{\rm NS},T}^n=\frac{\bar{B}_{{\rm NS},T}^n}{1+\bar{\gamma}_{\rm NS}^{0,n}/2\beta_0}-\frac{\bar{\gamma}_{\rm NS}^{1,n}+2\beta_1}{\bar{\gamma}_{\rm NS}^{0,n}(1+\bar{\gamma}_{\rm NS}^{0,n}/2\beta_0)}, \quad (4.17)$$

$$\bar{\Delta}_n=\bar{\gamma}_{G\psi}^{1,n}\bar{\gamma}_{\psi G}^{0,n}-\bar{\gamma}_{\psi\psi}^{1,n}\bar{\gamma}_{GG}^{0,n}+\frac{\bar{\gamma}_{G\psi}^{0,n}\bar{\gamma}_{\psi G}^{1,n}\bar{\gamma}_{GG}^{0,n}+\bar{\gamma}_{GG}^{0,n}\bar{\gamma}_{G\psi}^{1,n}\bar{\gamma}_{\psi G}^{0,n}-\bar{\gamma}_{\psi G}^{0,n}\bar{\gamma}_{GG}^{1,n}\bar{\gamma}_{G\psi}^{0,n}-\bar{\gamma}_{GG}^{0,n}\bar{\gamma}_{\psi\psi}^{1,n}\bar{\gamma}_{GG}^{0,n}}{2\beta_0}. \quad (4.18)$$

The Eq. (4.11) for the leading term $\bar{a}_n$ is valid for $n\geq 2$, and agrees with the results of Refs. 3 and 7. The Eqs. (4.12) and (4.13) are valid for $n>2$. For $n=2$, $\bar{\lambda}_-^2$ vanishes and we cannot evaluate the constant term $\bar{b}_2$, since this constant term depends on the unknown fermion and gluon renormalized cut vertices. For $\bar{a}_2'$ we obtain

$$\bar{a}_2'=\frac{\beta_1}{\beta_0^2}\bar{a}_2+\frac{1}{2\bar{\lambda}_+\beta_0}\left\{\delta_\psi[\bar{K}_\psi^1\bar{\gamma}_{\psi\psi}^0-\bar{K}_G^1\bar{\gamma}_{\psi G}^0]+\frac{\bar{\Delta}}{\bar{d}}-\frac{\beta_1}{\beta_0}\bar{K}_\psi^0\delta_\psi\bar{\gamma}_{GG}^0\right\}, \quad (4.19)$$

where $\bar{a}_2$ is evaluated from (4.11) and the index $n=2$ has been dropped in the second term. The Eqs. (4.12), (4.13), and (4.19) are new results.

The parton model predicts for the asymptotic behavior of the moments $\bar{W}_T^\gamma$ from Eq. (1.8) as

$$\int_0^1 dz\, z^n\bar{W}_T^\gamma(z,q^2)\big|_{\rm PM}=\alpha^2\bar{p}_n\ln\frac{q^2}{\Lambda_{\rm PM}^2}, \quad (4.20)$$

where

$$\bar{p}_n=4\delta_\gamma\frac{n^2+n+2}{(n-1)n(n+1)} \quad (4.21)$$

and m_q^2 has been replaced by a mass parameter $\Lambda_{\rm PM}^2$. The above PM prediction is also obtained from Eq. (4.11) if all anomalous dimensions except $\bar{K}_\psi^{0,n}$ and $\bar{K}_{\rm NS}^{0,n}$ are set equal to zero.

We give in Table II the numerical values for the parameters $\bar{a}_n$, $\bar{a}_n'$, $\bar{b}_n$, and $\bar{p}_n$ as functions n in the case of four flavors. For increasing n, $\bar{a}_n$ decreases faster to zero than $\bar{p}_n$. In fact $\bar{a}_n$ vanishes as $1/(n\ln n)$ for large n, while $\bar{p}_n$ behaves as $1/n$. Therefore, the photon structure function $\bar{W}_T^\gamma(z,q^2)$ as given by the leading-order expression is suppressed at large values of z as compared with the parton model predictions. The large negative value of $\bar{a}_2'$ is due to large negative values of $\bar{K}_\psi^{1,2}$ and $\bar{K}_G^{1,2}$.

The parameters $\bar{b}_n$ are negative and large. They decrease with increasing n slightly faster than $\bar{a}_n$, but still remain large relative to $\bar{a}_n$. In Table III we list the ratio of $\bar{b}_n$ to $\bar{a}_n$ as functions of n, and also the corresponding ratio b_n/a_n in the case of the photon structure function F_2^γ in the photon-photon scattering. Note that these values have been calculated in the $\overline{\rm MS}$ scheme. In comparison with the case of F_2^γ, the higher-order corrections to the timelike photon structure function $\bar{W}_T^\gamma$ are very large.

Now we evaluate the moments of $\bar{W}_T^\gamma$. We shall take $\Lambda=0.30$ GeV as a "standard" value in the $\overline{\rm MS}$ scheme.[25] In Fig. 6 we plot the moments of $\bar{W}_T^\gamma$ in units of $\alpha^2\ln(Q^2/\Lambda^2)$ as predicted by the parton model, by QCD in the leading order, and by QCD

TABLE II. Numerical values of the parameters $\bar{a}_n$, $\bar{a}_n'$, $\bar{b}_n$, and $\bar{p}_n$ for $f=4$.

n	$\bar{a}_n$	$\bar{a}_n'$	$\bar{b}_n$	$\bar{p}_n$
2	4.98	−4.99		6.72
4	1.01	0.745	−6.95	1.85
6	0.508	0.375	−3.14	1.06
8	0.328	0.243	−1.92	0.740
10	0.238	0.176	−1.35	0.570
12	0.185	0.137	−1.02	0.464
14	0.150	0.111	−0.818	0.391
16	0.126	0.0932	−0.676	0.338
18	0.018	0.0799	−0.574	0.298
20	0.0944	0.0698	−0.497	0.266

TABLE III. Numerical values of the ratios $\bar{b}_n/\bar{a}_n$ and b_n/a_n. The ratios b_n/a_n in photon-photon scattering have been calculated from the results of Ref. 2.

n	$\bar{b}_n/\bar{a}_n$	b_n/a_n
4	−6.88	−2.04
6	−6.18	−2.26
8	−5.85	−2.44
10	−5.67	−2.59
12	−5.51	−2.70
14	−5.45	−2.81
16	−5.37	−2.89
18	−5.31	−2.95
20	−5.26	−3.01

with higher-order corrections. From Fig. 6 it is seen that QCD higher-order effects are significant. The substantial suppressions of the first few moments are due to the large negative values of $\bar{b}_n$. For example, the moment of $n=4$ almost vanishes at $q^2=25$ GeV^2 and indeed it turns out to be negative at $q^2=20$ GeV^2.

This may suggest that even at $q^2=20$ GeV^2 the contributions from the hadronic nature of the photon, which vanish for large q^2 as $(\ln q^2/\Lambda^2)^{-h}$ with some positive constant h and so far have been neglected, are still significant, or that the QCD calculation for the direct photon production in e^+e^- annihilation breaks down.

The structure function for large-z values is governed by the large-n behavior of the moments. The asymptotic behavior of $\bar{a}_n$ is $1/(n\ln n)$. From Eq. (4.13) we find the parameter $\bar{b}_n$ behaves as $1/n$, but not as $\ln n/n$ for large n. In fact the contribution from the first four terms in Eq. (4.13) to $\bar{b}_n$

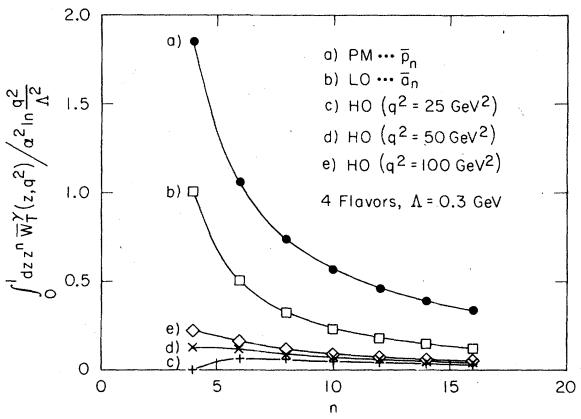

FIG. 6. Moments of the transverse structure function $\bar{W}_T^\gamma$ in units of $\alpha^2\ln q^2/\Lambda^2$ as predicted by the parton model (a); QCD in the leading order (LO) (b), and QCD with the higher-order (HO) corrections (c), (d), and (e). For comparison we choose $\Lambda=0.3$ GeV and four flavors for all cases.

behaves as $\ln n/n$. However, the last term $\bar{B}_\gamma^n\delta_\gamma$ behaves also as $\ln n/n$ in the large-n limit with the same coefficient but the opposite sign, and it cancels the leading contribution from the first four terms. Therefore the ratio $\bar{b}_n/\bar{a}_n$ grows not as $(\ln n)^2$ but as $\ln n$.[26] This is also the case for the moments of the photon structure function F_2^γ. The situation here is quite different from cases of deep-inelastic scatterings off hadronic targets and semi-inclusive hadron productions in e^+e^- annihilation. For instance, the moments of nonsinglet nucleon structure function in deep-inelastic scattering can be written generally as

$$M_n(Q^2)=A_n\left(\frac{\bar{g}^2}{16\pi^2}\right)^{\gamma_{\rm NS}^{0,n}/2\beta_0}\left(1+\frac{\bar{g}^2}{16\pi^2}R_n\right), \qquad (4.22)$$

where A_n is the matrix element of the nonsinglet operators. The higher-order correction R_n has been calculated[11,21] and grows as $(\ln n)^2$ for large n. In the case of the moments of $\bar{W}_T^\gamma$ (F_2^γ), the corresponding quantity to R_n in Eq. (4.22) is $\beta_0\bar{b}_n/\bar{a}_n$ ($\beta_0 b_n/a_n$). It behaves as $\ln n$ in the large-n limit, since cancellation occurs among its leading $(\ln n)^2$ terms. The pointlike nature of the photon plays an important role for the cancellation of leading $(\ln n)^2$ terms.

Finally, a few comments are in order. The mass effects due to heavy quarks have not been taken into account in our formulas for the moments of $\bar{W}_T^\gamma$. The quantities necessary to evaluate $\bar{a}_n$, $\bar{a}_n'$, and $\bar{b}_n$ have been calculated for arbitrary f-quark flavors with all quark masses zero, and the results have been presented for $f=4$ only. Up to $q^2=20$ GeV^2 mass effects due to charm production could be important. As q^2 increases the charm-quark mass effects may be neglected. And we expect that our predictions for four flavors are valid in the range of q^2 from 25 GeV^2 up to 100 GeV^2. Above $q^2\approx 100$ GeV^2 the b-quark contribution should be added, but it is small compared with the charm contribution by a factor of 16 due to its charge.

Secondly, the expressions of the two-loop anomalous dimensions given in Sec. III B are valid for even values of n. In fact, taking moments of the two-loop parton probability functions with arbitrary n, we find that the anomalous dimensions can be written in the following form[17,21,27]:

$$\gamma^{1,n}=\gamma_n^A+(-1)^n\gamma_n^B\,. \qquad (4.23)$$

The expressions in Sec. III B have been obtained by taking the (+) combination, i.e., $\gamma_n^A+\gamma_n^B$. Because of the crossing relation for the structure function $\bar{W}_T^\gamma$, the (+) combination should be adopted here and it can be analytically continued to any value of n. Therefore, expressions (3.16)–(3.35) for two-loop anomalous dimensions can be also

used to compute b_n for odd values of n.

Thirdly, we have so far used the $\overline{\text{MS}}$ scheme. Since our perturbative expansion is a truncated one, its rate of convergence depends on the scheme used to define the running coupling constant $\bar{g}$.[11,28] We can change schemes by changing Λ and $\bar{b}_n$ as follows:

$$\Lambda \to \Lambda' = \kappa\Lambda ,$$
$$\bar{b}_n \to \bar{b}_n' = \bar{b}_n + a_n \ln\kappa^2 . \tag{4.24}$$

With the choice $\kappa = 2.16$, we can obtain the results for the momentum-space subtraction (MOM) scheme.[28] We give in Table IV the numerical values for $\bar{b}_n^{\text{MOM}}$ and the ratio $\bar{b}_n^{\text{MOM}}/\bar{a}_n$. In Fig. 7 we take[25] $\Lambda_{\text{MOM}} = 0.55$ GeV and plot the QCD predictions for the moments of $\overline{W}_T^\gamma$ in the MOM scheme. The values of $\bar{b}_n^{\text{MOM}}$ and $\bar{b}_n^{\text{MOM}}/\bar{a}_n$ have become smaller than those in the $\overline{\text{MS}}$ scheme, but the higher-order corrections are still large.

V. LONGITUDINAL PHOTON STRUCTURE FUNCTION $\overline{W}_L^\gamma$

The QCD prediction for the longitudinal photon structure function $\overline{W}_L^\gamma$ has not been considered so far, since it is expected that $\overline{W}_L^\gamma$ gives a small contribution to the direct photon production cross section. We proceed with the same steps of Sec. IV and expand $\vec{\mathbf{E}}_{L,n}(1, \bar{g}^2, \alpha)$ as follows:

$$E_{L,n}^i(1,\bar{g}^2,\alpha) = \begin{cases} e^2\delta_\psi \dfrac{\bar{g}^2}{16\pi^2}\bar{B}_{\psi,L}^n , & i=\psi, \quad (5.1)\\ e^2\delta_\psi \dfrac{\bar{g}^2}{16\pi^2}\bar{B}_{G,L}^n , & i=G, \quad (5.2)\\ e^2\delta_{\text{NS}} \dfrac{\bar{g}^2}{16\pi^2}\bar{B}_{\text{NS},L}^n , & i=\text{NS}, \quad (5.3)\\ \dfrac{e^4}{16\pi^2}\delta_\gamma \bar{B}_{\gamma,L}^n , & i=\gamma . \quad (5.4) \end{cases}$$

We obtain the one-loop corrections to $E_{L,n}^i(1, \bar{g}^2, \alpha)$ by taking moments of the relevant short-distance cross sections which have been calculated in Ref. 20. They are

TABLE IV. Numerical values of $\bar{b}_n^{\text{MOM}}$ and the ratio $\bar{b}_n^{\text{MOM}}/\bar{a}_n$ for $f=4$ in the MOM scheme.

n	$\bar{b}_n^{\text{MOM}}$	$\bar{b}_n^{\text{MOM}}/\bar{a}_n$
4	−5.39	−5.34
6	−2.36	−4.64
8	−1.41	−4.31
10	−0.983	−4.13
12	−0.735	−3.97
14	−0.587	−3.91
16	−0.482	−3.83
18	−0.408	−3.77
20	−0.352	−3.72

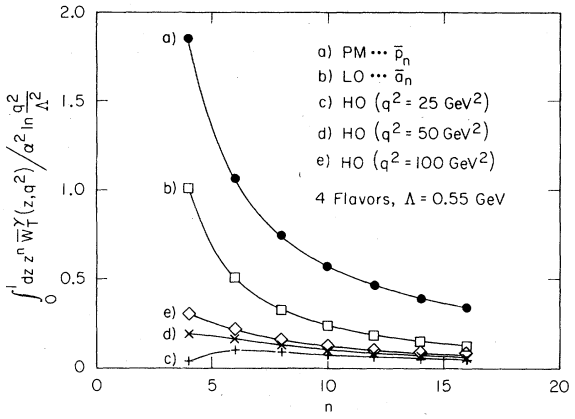

FIG. 7. Predictions of the MOM scheme for the moments of $\overline{W}_T^\gamma$ (c), (d), and (e) in units of $\alpha^2 \ln q^2/\Lambda^2$. Also shown for comparison are the results of the parton model (a), and QCD in the leading order (b). We choose $\Lambda = 0.55$ GeV and four flavors for all cases.

$$\bar{B}_{\psi,L}^n = \bar{B}_{\text{NS},L}^n = \frac{4}{3}\frac{4}{n} , \tag{5.5}$$

$$\bar{B}_{G,L}^n = \frac{8f}{(n-1)n} , \tag{5.6}$$

$$\bar{B}_{\gamma,L}^n = \frac{2\bar{B}_{G,L}^n}{f} . \tag{5.7}$$

The above results are renormalization-prescription independent, since no renormalization is needed for the calculation of the one-loop corrections to $\vec{\mathbf{E}}_{L,n}(1, \bar{g}^2, \alpha)$.

The moments of $\overline{W}_L^\gamma$ can be obtained from Eqs. (4.13), (4.16), and (4.17) by putting there all two-loop contributions to zero and replacing the parameters $\bar{B}_{i,T}^n$ by $\bar{B}_{i,L}^n$. As the result we obtain

$$\int_0^1 dz\, z^n \overline{W}_L^\gamma(z,q^2) = \alpha^2 \bar{c}_n + O(\bar{g}^2) , \tag{5.8}$$

where

$$\bar{c}_n = \frac{1}{2\beta_0}(\bar{K}_\psi^{0,n}\delta_\psi \bar{R}_{\psi,L}^n + \bar{K}_{\text{NS}}^{0,n}\delta_{\text{NS}}\bar{R}_{\text{NS},L}^n) + \delta_\gamma \bar{B}_{\gamma,L}^n \tag{5.9}$$

and

$$\bar{R}_{\psi,L}^n = \frac{\bar{B}_{\psi,L}^n}{\bar{d}_n}\left(1 + \frac{\bar{\gamma}_{GG}^{0,n}}{2\beta_0}\right) - \frac{\bar{B}_{G,L}^n}{\bar{d}_n}\frac{\bar{\gamma}_{G\psi}^{0,n}}{2\beta_0} , \tag{5.10}$$

$$\bar{R}_{\text{NS},L}^n = \frac{\bar{B}_{\text{NS},L}^n}{1 + \bar{\gamma}_{\text{NS}}^{0,n}/2\beta_0} , \tag{5.11}$$

and $\bar{d}_n$ is given by Eq. (4.15).

From Eq. (1.9) the parton model predicts for the moments of $\overline{W}_L^\gamma$

$$\int_0^1 dz\, z^n \overline{W}_L^\gamma(z,q^2)\big|_{\text{PM}} = \alpha^2 \bar{c}_{n,\text{PM}} , \tag{5.12}$$

where

$$\bar{c}_{n,\text{PM}} = \delta_\gamma \bar{B}_{\gamma,L}^n . \tag{5.13}$$

TABLE V. Numerical values for the parameters $\bar{c}_n$ and $\bar{c}_{n,\mathrm{PM}}$ for $f=4$.

n	$\bar{c}_n$	$\bar{c}_{n,\mathrm{PM}}$
2	12.2	10.1
4	1.85	1.68
6	0.726	0.672
8	0.386	0.360
10	0.239	0.224
12	0.163	0.153
14	0.118	0.111
16	0.0890	0.0840
18	0.0697	0.0658
20	0.0560	0.0530

For the longitudinal structure function, both QCD and the parton model predict scaling. Numerical values for $\bar{c}_n$ and $\bar{c}_{n,\mathrm{PM}}$ are given in Table V.

We find that the numerical values of $\bar{c}_n$ are very close to $\bar{c}_{n,\mathrm{PM}}$. For large n the difference $\bar{c}_n - \bar{c}_{n,\mathrm{PM}}$ vanishes as $1/(n^2 \ln n)$. This means that the renormalization effects as given by the first two terms in Eq. (5.9) are small. In consequence, except for very small z, QCD gives the shape of $\bar{W}_L^\gamma$ very similar to that obtained in the parton model. Similar predictions had been made for the longitudinal photon structure function F_L^γ in photon-photon scattering[1,2]: The renormalization effects of QCD on F_L^γ are small, and the parton model and QCD predict a similar shape for F_L^γ.

VI. SUMMARY AND COMMENTS

In this paper we have analyzed in QCD the photon structure functions $\bar{W}_T^\gamma$ and $\bar{W}_L^\gamma$ which can be observed in direct photon production in e^+e^- collisions. We have used Mueller's cut-vertex formalism and have introduced the bare cut vertex for two photons in addition to the usual fermion and gluon cut vertices. The two-loop anomalous dimensions of cut vertices have been calculated by taking moments of the two-loop parton decay probability functions. The $\bar{g}^2$ corrections to the coefficient functions $\tilde{\mathbf{E}}_{k,n}(1, \bar{g}^2, \alpha)$ in Eq. (2.21) have also been calculated. With this information and with the already known one-loop anomalous dimensions of cut vertices, we have evaluated the next-to-leading-order corrections to $\bar{W}_T^\gamma$ and the leading-order corrections to $\bar{W}_L^\gamma$. The higher-order corrections to $\bar{W}_T^\gamma$ are found to be considerably large and to be much larger than those to F_2^γ in deep-inelastic photon-photon scattering. On the other hand, the leading-order corrections to $\bar{W}_L^\gamma$ are small. QCD and the parton model give a very similar shape for $\bar{W}_L^\gamma$.

Finally we comment on the backgrounds to direct photon production. First there is a large yield of photons from π^0 (and η) mesons which are produced in e^+e^- collisions. When we compare the QCD predictions for the direct photon production with experimental data, we need to somehow subtract photons coming from π^0. This subtraction is in principle possible if we have detailed data on the π^0 production in e^+e^- collisions. The ratio of the direct photon to π^0 production in e^+e^- annihilation has been considered by Koller *et al.*[7] They have used the QCD formulas for fragmentation functions to photon and π^0 calculated in the leading order with appropriate assumptions. They have found that the γ/π^0 ratio grows with q^2 owing to the logarithmic increase of the photon yield combined with the logarithmic decrease of the π^0 yield. Also the ratio sharply rises with z. The photons from π^0's tend to be softer than the direct ones. At PEP-PETRA energies the yield of hard direct photons is expected to be larger than the π^0 yield and the separation of the photons from π^0 (and η) mesons becomes feasible.

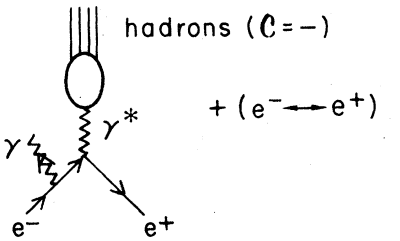

FIG. 8. Photon bremsstrahlung off electrons and positrons.

Another significant background to direct photon production arises from the "bremsstrahlung" process in Fig. 8, where the photon is emitted from an initial lepton rather than from a final quark line. However, as stated in Ref. 7 the photons from the bremsstrahlung process and the direct photons have different angular correlations with the e^+e^- beam axis and the quark-jet directions. This background can be quantitatively estimated and can thus be subtracted.

ACKNOWLEDGMENTS

It is my pleasure to thank Sid Drell for warm hospitality extended to me at SLAC. I have benefited from discussion with many people including W. A. Bardeen, A. J. Buras, S. J. Brodsky, S. Gupta, J. Kodaira, T. Muta, and L. Trentadue. I wish to thank S. Parke for advice and help in some of the calculations and for his personality which has made my stay at SLAC enjoyable. Finally, I acknowledge the financial support of the Nishina Memorial Foundation. This work was also supported by the Department of Energy under Contract No. DE-AC03-76SF00515. Some calculations have been done using the MIT computer MACSYMA.

*On leave of absence from the Department of Physics, Yokohama National University, Japan.
[1]E. Witten, Nucl. Phys. B120, 189 (1977).
[2]W. A. Bardeen and A. J. Buras, Phys. Rev. D 20, 166 (1979).
[3]C. H. Llewellyn Smith, Phys. Lett. 79B, 83 (1978).
[4]R. J. DeWitt, L. M. Jones, J. D. Sullivan, D. W. Willen, and H. W. Wyld, Jr., Phys. Rev. D 19, 2046 (1979); W. R. Frazer and J. F. Gunion, *ibid.* 20, 147 (1979); S. J. Brodsky, T. DeGrand, J. F. Gunion, and J. Weis, Phys. Rev. Lett. 41, 672 (1978); Phys. Rev. D 19, 1418 (1979); S. J. Brodsky, in *Jets in High Energy Collisions*, proceedings of the Copenhagen Symposium, 1978 (Royal Swedish Academy of Sciences, Stockholm, 1979), p. 154; K. Kajantie, Helsinki Report No. NU-TFT-78-30, 1978 (unpublished); D. W. Duke and J. F. Owens, Phys. Rev. D 22, 2280 (1980).
[5]M. A. Ahmed and G. G. Ross, Phys. Lett. 59B, 369 (1975); F. Delduc, M. Gourdin, and E. G. Oudrhiri-Safiani, Nucl. Phys. B174, 147 (1980); B174, 157 (1980); C. Peterson, T. F. Walsh, and P. M. Zerwas, *ibid.* B174, 424 (1980); W. R. Frazer and G. Rossi, Phys. Rev. D 21, 2710 (1980); K. Sasaki, *ibid.* 22, 2143 (1980); A. C. Irving and D. B. Newland, Z. Phys. C 6, 27 (1980); A. Vourdas, J. Phys. G 6, 789 (1980).
[6]T. F. Walsh and P. Zerwas, Phys. Lett. 44B, 195 (1973).
[7]K. Koller, T. F. Walsh, and P. M. Zerwas, Z. Phys. C 2, 197 (1979).
[8]N. Kai, H. Yamamoto, and K. Kato, Tokyo Report No. UT-341, 1980 (unpublished).
[9]G. Altarelli and G. Parisi, Nucl. Phys. B126, 298 (1977).
[10]M. Bacé, Phys. Lett. 78B, 132 (1978).
[11]W. A. Bardeen, A. J. Buras, D. W. Duke, and T. Muta, Phys. Rev. D 18, 3998 (1978).
[12]A. H. Mueller, Phys. Rev. D 18, 3705 (1978).
[13]S. Gupta and A. H. Mueller, Phys. Rev. D 20, 118 (1979); S. Gupta, Phys. Rev. D 21, 984 (1980).
[14]We define $p_\pm = (1/\sqrt{2})(p_0 \pm p_3)$.
[15]D. R. T. Jones, Nucl. Phys. B74, 531 (1974); W. Caswell, Phys. Rev. Lett. 33, 244 (1974).
[16]J. F. Owens, Phys. Lett. 76B, 85 (1978); T. Uematsu, Phys. Lett. 79B, 97 (1978); H. Georgi and H. D. Politzer, Nucl. Phys. B136, 445 (1978); Yu. L. Dokshitser, D. I. Dyakanov, and S. I. Troyan, Report No. SLAC-TRANS-183, 1978 (unpublished).
[17]G. Curci, W. Furmanski, and R. Petronzio, Nucl. Phys. B175, 27 (1980); W. Furmanski and R. Petronzio, Phys. Lett. 97B, 437 (1980).
[18]E. G. Floratos, R. Lacaze, and C. Kounnas, Phys. Lett. 98B, 89 (1981); 98B, 285 (1981).
[19]J. Kalinowski, K. Konishi, and T. R. Taylor, Nucl. Phys. B181, 221 (1981); J. Kalinowski, K. Konishi, R. N. Scharbach, and T. R. Taylor, *ibid.* B181, 253 (1981).
[20]G. Altarelli, R. K. Ellis, G. Martinelli, and So-Young Pi, Nucl. Phys. B160, 301 (1979).
[21]E. G. Floratos, D. A. Ross, and C. T. Sachrajda, Nucl. Phys. B129, 66 (1977); B139, 545 (1978); B152, 493 (1979).
[22]G. 't Hooft, Nucl. Phys. B61, 455 (1973).
[23]Our definition of nondiagonal elements differs by a sign from that of Eq. (14) in Ref. 17.
[24]A. Gonzalez-Arroyo, C. Lopez, and F. J. Yndurain, Nucl. Phys. B153, 161 (1979); A. Gonzalez-Arroyo and C. Lopez, Nucl. Phys. B166, 429 (1980).
[25]A. J. Buras, Fermilab Report No. FERMILAB-CONF-80/79-THY (unpublished).
[26]The increase of the ratio $\bar{b}_n/\bar{a}_n$ with n has not shown itself in Table III yet.
[27]D. A. Ross and C. T. Sachrajda, Nucl. Phys. B149, 497 (1979).
[28]W. Celmaster and R. J. Gonsalves, Phys. Rev. Lett. 42, 1435 (1979); Phys. Rev. D 20, 1420 (1979); W. Celmaster and D. Sivers, *ibid.* 23, 227 (1981).